Development of a compact ICRF antenna for high-power and long-pulse plasma heating in the KSTAR

Kenji Saito[a,b,*], Hyunho Wi[c], Sonjong Wang[c], Haejin Kim[d], Kwangho Jang[c], Hyunyeong Lee[c], Jeehyun Kim[c], and Jong-Gu Kwak[c]

[a] *National Institute for Fusion Science, National Institutes of Natural Sciences, Toki, Gifu 509-5292, Japan*
[b] *Department of Fusion Science, The Graduate University for Advanced Studies, SOKENDAI, Toki, Gifu 509-5292, Japan*
[c] *National Fusion Research Institute, 169-148, Gwahak-ro, Yuseong-gu, Daejeon 34133, Korea*
[d] *ITER Organization, Route de Vinon-sur-Verdon, CS 90 046, 13067 St Paul Lez Durance Cedex, France*

For the high-power and long-pulse ion cyclotron range of frequencies (ICRF) heating of the KSTAR plasma, we developed the compact ICRF antenna (CIA). The target injection power of CIA is 2 MW for 300 s. In order to continue injecting the power into plasma even if drastic instantaneous changes occur in the plasma condition, such as ELM events, we adopted the internal conjugate-T method for the load resilience. Between antenna heads and the junction point, impedance transformers were inserted to satisfy the condition of conjugate-T in a limited space keeping the electric field on the transformer low enough. To reduce the risk of water leakage into the vacuum chamber, only the backsides of antenna heads are water-cooled in the in-vessel region.

Keywords: ICRF heating; conjugate-T; impedance transformer; CIA; KSTAR

1. Introduction

Ion Cyclotron Range of Frequencies (ICRF) heating has been conducted in the Korea Superconducting Tokamak Advanced Research (KSTAR) [1] using the ICRF antenna with four center-grounded current straps [2]. However, this antenna suffered frequent damage by arcing on the ceramic feedthroughs [3]. Therefore, the ICRF antenna was removed from the KSTAR, and a port for a new ICRF antenna was allocated. However, the port width is approximately one-half of that of the former ICRF antenna. Therefore, development of Compact ICRF Antenna (CIA) was required.

In the KSTAR, there is one high-performance transmitter [4], which has been used for the former ICRF antenna. By connecting this transmitter to the liquid dummy load [5], the injection power of 1.9 MW for 300 s was achieved, where the injection time of 300 s is the specified maximum duration time of the long-pulse operation in the KSTAR. Therefore, the target power and the injection time for the CIA design were set to 2 MW and 300 s, respectively.

Conjugate-T is a method which reduces the reflection even in ELMy H-mode plasma [6,7]. At the end of one transmission line, two transmission lines with different line lengths are connected and the opposite ends of the lines are connected to antenna heads. By choosing the proper line lengths, it would be possible to have the same impedance at the input port with the two different antenna loading resistances. As a result, the reflection coefficient is kept low in a wide region of antenna impedance. This technique was generalized and incorporated in the design of CIA.

Also in the Large Helical Device (LHD) [8], ICRF heating has been conducted and numerous physical facts regarding ICRF heating were revealed [9]. Moreover, ICRF heating has been playing an important role in long pulse operations [10,11]. The ceramic feedthrough for ICRF heating in the LHD [12] is larger and less damaged by arcing compared to that for the former ICRF antenna in the KSTAR. Therefore, the LHD-type feedthrough was determined to be used in the CIA. Field-Aligned-Impedance-Transforming (FAIT) antenna [13] in the LHD has the optimized in-vessel impedance transformer [14] in order to reduce VSWR in the transmission line with protecting the ceramic feedthrough and keeping the electric field in the impedance transformer low. This technique was also incorporated in the development of CIA.

The main requirements for the design of CIA are listed as follows:

- Compactness
- High heating efficiency
- Injection power of 2 MW for 300 s
- Load resilience with conjugate-T
- Keeping electric field low enough in the entire system
- Minimizing the risk of water leakage

In Section 2, the design of CIA is described including the antenna head design, the calculation method of generalized conjugate-T, the improvement of the optimization method of impedance transformer, the combination of the conjugate-T and the impedance transformer, and the design of impedance matching unit. In Section 3, results of electromagnetic simulations will be shown. Section 4 summarizes the work.

2. Design of CIA

Fig. 1(a) and (b) show the entire structure of CIA and the cross section, respectively. CIA consists of the vertically aligned antenna heads, the in-vessel impedance transformers, the junction unit, the ceramic feedthrough, and the impedance matching unit. In order to support inner conductor in the junction unit, a ceramic disk is inserted just below the junction point, where the voltage

* Corresponding author.
E-mail address: saito@nifs.ac.jp (Kenji Saito).

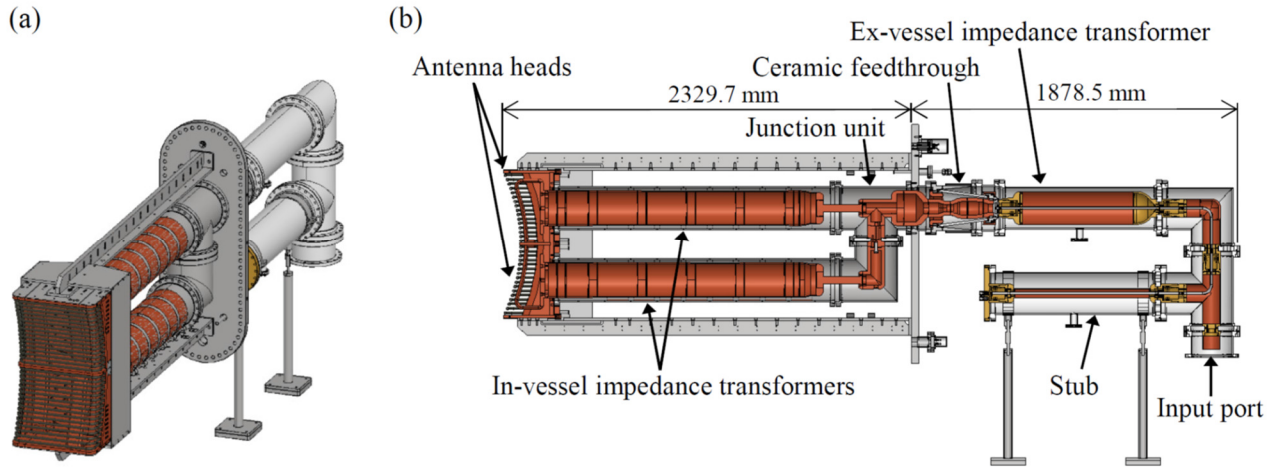

Fig. 1 (a) Entire structure of CIA. (b) Cross section of CIA.

is low enough. Outer conductors in in-vessel region are made with stainless steel coated with copper on the inner surface and outer conductors in ex-vessel region are made with aluminum. Brown and yellow parts are made with copper and brass, respectively. The front surface of Faraday shield is retreated by 1 cm from the front surface of limiters to the radial direction for the protection of the antenna.

2.1 Design of antenna head of CIA

Operation frequency of the ICRF heating was fixed at 30.8 MHz in the KSTAR. In this frequency, the ion cyclotron resonance layer of hydrogen locates in the place where the magnetic field strength is 2.02 T. At the configuration where the resonance layer locates in the plasma core, minority ion heating of hydrogen and second harmonic heating of deuterium are expected as an intense heating method. For the high heating efficiency which is defined as the absorbed power normalized by the injection power, a large wave number parallel to the static magnetic field $k_{//}$ is necessary, especially for the minority ion heating because of the large Doppler broadening of the resonance layer into the region where the left-hand polarized electric field is sufficient. Therefore, each antenna head has two straps and the current directions in each strap are opposite (0-π current phasing) as shown in Fig. 2. High $k_{//}$ is preferable for the high heating efficiency. However, it leads to the low coupling since the density at the right-hand cutoff layer is high and the position of the cutoff layer is far from the antenna. Therefore, in the design of CIA, the distance between straps in each antenna head was maximized within the port width of 314 mm in order to reduce $k_{//}$. Each strap width is 86 mm and the distance between two straps in each antenna head is 128 mm. Then, the peak toroidal wave number in front of antenna heads ($\approx k_{//}$) is deduced as 13.9 m^{-1} with the model of constant current density on the straps. Since the width of the Faraday shield is larger than the port width, the Faraday shield will be attached to the antenna heads at the inside of the vacuum vessel after the installation of the antenna. To minimize the risk of water leakage, antenna heads are indirectly water-cooled with the cooling blocks attached to the backsides of antenna heads. For the heat removal with the thermal conductivity, antenna heads were made with copper and Faraday shields were coated with tungsten to avoid spattering by the plasma.

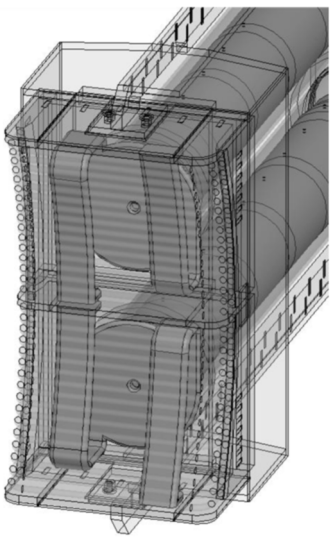

Fig. 2 Antenna heads of CIA with double straps. Each center disk has two straps connected to the antenna box.

2.2 Design method of generalized conjugate-T

For the condition of conjugate-T, proper impedance conversion is necessary between antenna heads and the junction point with the limited spaces. Therefore, we used impedance transformers. We treat the antenna property in general. That is, not only antenna loading resistance but also other parameters are incorporated in the calculation by using scattering matrix (S-matrix) of the antenna heads S_a. Here, we describe the calculation method for the proper extra line lengths between the impedance transformers and the junction unit with the given two different S-matrices of the antenna heads.

Fig. 3 shows the schematic diagram of the conjugate-T system. S-matrix of the two identical impedance transformers S_t and that of the junction unit S_j are given. Impedance matching at the input port (port 3) is assumed to be performed at the S-matrix of the antenna heads of S_{a1}. To keep the reflected power zero even if the plasma

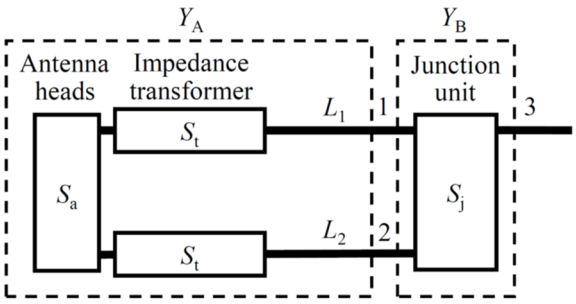

Fig. 3 Schematic diagram of the conjugate-T system for CIA.

condition changes, that is, the S-matrix of the antenna heads changes from S_{a1} to S_{a2}, the following conjugate-T condition must be satisfied:

$$y(S_{a1}, L_1, L_2) = y(S_{a2}, L_1, L_2), \tag{1}$$

where y notes the admittance at the port 3 and L_1, L_2 are lengths of extra lines inserted between impedance transformers and the junction unit. Since real and imaginary parts exist in Eq. (1), extra line lengths L_1 and L_2 can be solved. The admittance y at the input port is calculated with the procedure mentioned in Appendix A.

2.3 Design method of optimized impedance transformer

In the LHD, impedance transformers were designed by giving the impedance at the outlet z_a so as to minimize the VSWR on the transmission line with the limitation of the current and the voltage at the ceramic feedthrough and the electric field on the impedance transformer within the allowable level [14]. Here in the design of CIA, we must satisfy the conjugate-T condition. Therefore, instead of minimization of VSWR on the transmission line, electric field on the inner conductor of the impedance transformer was minimized with the condition that the complex reflection coefficient at the inlet of the impedance transformer Γ is the same with the target value Γ_0 which will be deduced in the following Section 2.4 with the conjugate-T condition. The actual optimization was conducted as the following procedure:

(1) The inner conductor of the impedance transformer is divided into several segments as shown in Fig. 4 assuming cylindrical shape. The radii of inner conductors are independently and discreetly scanned to search the minimum $|\Gamma\text{-}\Gamma_0|$ with the constraint of $e<e_{th}$, where e is the maximum amplitude of the electric field on the inner conductor of the impedance transformer normalized by the root of the input power and e_{th} is a given threshold value. Electric field in transmission line is estimated at the center and at both ends in each segment.

(2) Near the optimum combination of the radii of inner conductors, scan ranges of radii are narrowed and the calculation is repeated several times in order to obtain the solution of $|\Gamma\text{-}\Gamma_0|=0$.

(3) Threshold e_{th} is gradually reduced until solution disappears, that is, $|\Gamma\text{-}\Gamma_0|$ does not converge to zero.

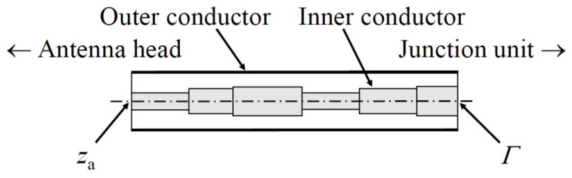

Fig. 4 Schematic drawing of the segmented impedance transformer.

2.4 Integration of the conjugate-T and the optimized impedance transformer

The operation region of S-matrix of the antenna heads was assumed as follows. Here, we define the S-matrix of the antenna heads with the port impedances of 50 Ω. By using HFSS (High Frequency Structure Simulator, ANSYS), loading resistances of the former ICRF antenna were calculated by locating the pseudo plasma away from limiters by 1 cm. When the pseudo plasma has the relative dielectric constant ε_r of 1.0×10^3, the calculated loading resistance of 1.2 Ω was the same with the typical experimental loading resistance for the H-mode plasma. Therefore, the material with $\varepsilon_r=1.0\times10^3$ was used as the typical plasma also for the CIA. The loading resistance of the antenna head R_a defined with the characteristic impedance z_c of 50 Ω at the backside of the antenna head was 1.7 Ω in the typical case. Minimum and maximum loading resistances of the antenna heads are also deduced with the former ICRF antenna data as 0.78 and 5.7 Ω, respectively. The impedance matching points where the reflected power to the transmitter side is zero were set at the loading resistances of antenna heads as 1.25 Ω (=R_{a1}) and 5.0 Ω (=R_{a2}). The loading resistances R_{a1} and R_{a2} were used in the calculation for the conjugate-T and the loading resistance R_{a1} was also used in the optimization of the impedance transformer. The experiments in the LHD revealed that the voltage distribution on the line connected to the antenna head shifts to the transmitter side with the loading resistance roughly by 1 cm/Ω with some scattering [15]. The value of the shift is adopted in the design of CIA to determine the phase of S_{a11} and S_{a22}. Because there are no experimental data on the mutual coupling terms S_{a12} and S_{a21}, these values were assumed to be identical, and the absolute value and the phase were set to 0.017 and 69°, respectively, according to the simulated result obtained by the pseudo plasma model with $\varepsilon_r=1.0\times10^3$ by using HFSS. These values were fixed even if the loading resistance changed.

By adding extra lines with the length of L_1 and L_2 calculated with Eq. (1), conjugate-T condition will be satisfied. However, here, the target reflection coefficient at the inlet of impedance transformer Γ_0 was adjusted instead of adding the extra lines because of the limited space for CIA. So as to make the extra line lengths L_1 and L_2 zero, Γ_0 was modified with the following equations:

$$\begin{cases} \phi_0' = \phi_0 - 2\pi(L_1 + L_2)/\lambda \\ R_0' = R_0 + (L_1 - L_2)/h, \end{cases} \tag{2}$$

where ϕ_0 and R_0 are the target phase of reflection coefficient and the loading resistance, respectively, at the inlet of impedance transformer where the characteristic

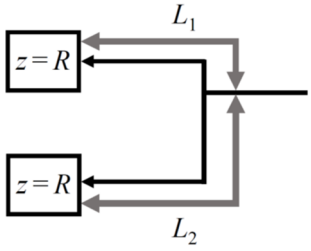

Fig. 5 Schematic diagram of the ideal conjugate-T model.

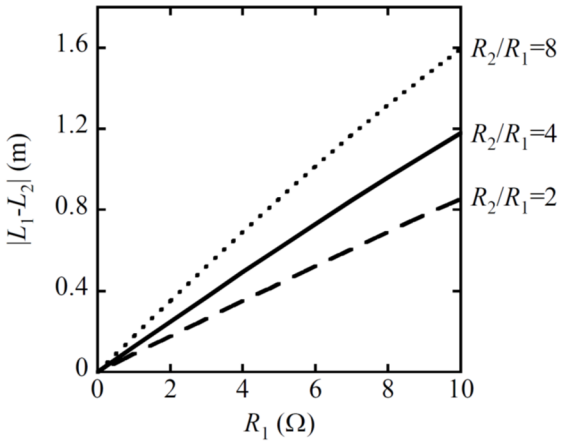

Fig. 6 The relation of difference of line lengths and the lower loading resistance for the impedance matching in the case of ideal conjugate-T model.

impedance z_c is assumed to be 50 Ω. The values after the modification are expressed by the prime (′). λ is the wavelength of 9.73 m, and h is the modification factor of the loading resistance obtained with the following ideal conjugate-T model. Fig. 5 shows the schematic diagram of the ideal conjugate-T model, where the mutual coupling of antenna heads is ignored and the lines are connected at a point. The characteristic impedance of lines is assumed to be 50 Ω and the impedance z at the two output ports is assumed to be real (z=R). When R takes values of R_1 and R_2 (R_1<R_2), impedance matching is performed. Fig. 6 shows the relations between the lower loading resistance R_1 and the difference of line lengths $|L_1$-$L_2|$ in the three case of R_2/R_1 calculated with the ideal conjugate-T model so as to satisfy the conjugate-T condition of Eq. (1). In general, the ratio of the loading resistances at the outlet of the impedance transformer R_{a2}/R_{a1} is almost the same with that at the inlet [15]. Therefore, R_2/R_1=5.0/1.25=4 was adopted for the determination of modification factor h and then the approximate relation of $|L_1$-$L_2|/R_1$=0.12 m/Ω was obtained. Therefore, the modification factor h was deduced to be 0.12 m/Ω. The impedance transformer is optimized with the modified target values at the inlet determined with Eq. (2) by giving the impedance at the outlet ignoring mutual coupling terms S_{a12} and S_{a21}. By using the S-matrix of the impedance transformer obtained with HFSS, where the model is smoothed to avoid the concentration of the electric field, the extra line lengths L_1 and L_2 are calculated using Eq. (1), where the characteristic impedance of the lines is assumed to be 50 Ω. These

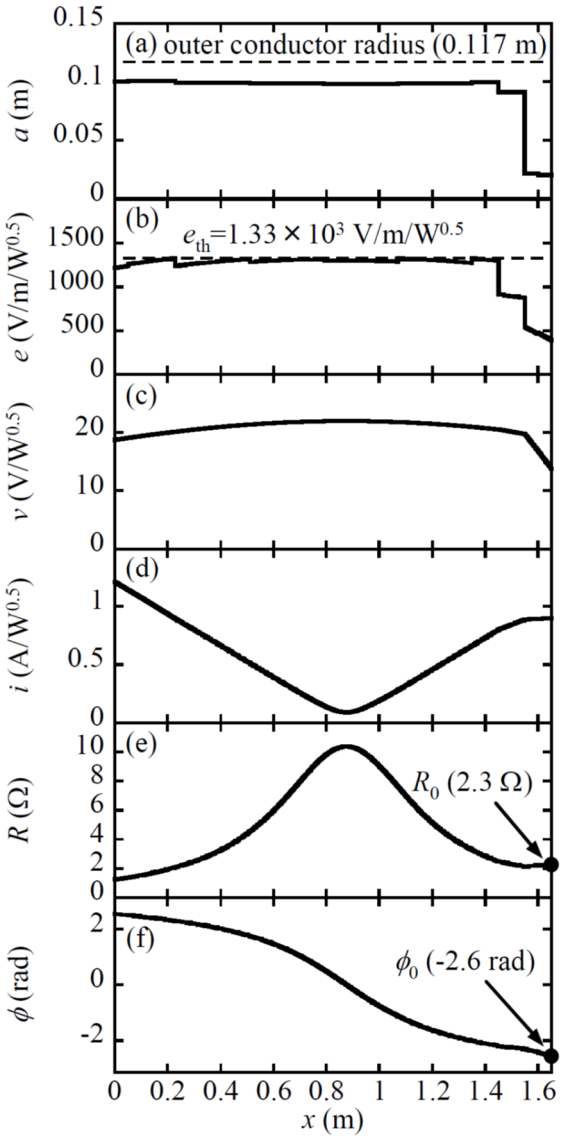

Fig. 7 The converged results on the optimized impedance transformer solved at one operation point of R_a=1.25 Ω without including mutual coupling for (a) the radius of inner conductor, (b) the normalized amplitude of the electric field on the inner conductor, (c) the normalized voltage, (d) the normalized current, (e) the loading resistance, and (f) the phase of reflection coefficient.

calculations are repeated until extra line lengths converge to zero. The converged results on the optimized impedance transformer are shown in Fig. 7. The amplitude of the electric field, the voltage, and the current are normalized by the root of the input power into the impedance transformer. The loading resistance R and the phase of reflection coefficient ϕ were estimated with the characteristic impedance of 50 Ω. The loading resistance R increases from the loading resistance at the antenna head of 1.25 Ω (=R_{a1}) to 10.4 Ω and drops to the target value of 2.3 Ω. Normally, the phase of reflection coefficient changes by 2π rad with the length of $\lambda/2$=4.87 m. However, by using this impedance transformer, the necessary length is shortened to approximately 40%. Therefore, these calculation methods worked well for the

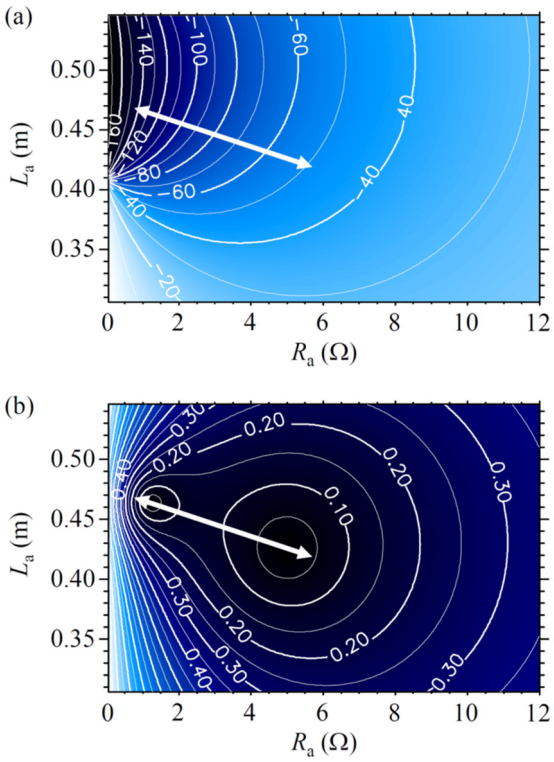

Fig. 8 Contour maps for (a) the phase of V_{f_bottom}/V_{f_top} in degrees and (b) the reflection coefficient $|V_r/V_f|$ in the R_a-L_a space.

compactness of CIA. This impedance transformer without extra lines satisfies the condition of conjugate-T expressed by Eq. (1) which includes the mutual coupling between antenna heads. However, the impedances at the top and bottom heads are assumed to be the same in the impedance transformer for Fig. 7. That is, the mutual coupling is ignored. Therefore, electromagnetic simulation that will be described in Section 3 is necessary for the precise estimation of the electromagnetic properties because of the existence of the mutual coupling. Fig. 8(a) and (b) show the contour maps of two major antenna properties in the R_a-L_a space, where S_{a11} and S_{a22} are defined with the following equation:

$$S_{a11} = S_{a22} = \frac{R_a - z_c}{R_a + z_c} \exp(-2jkL_a), \tag{3}$$

where the characteristic impedance z_c is assumed to be 50 Ω and wave number in the transmission line k is 0.65 m^{-1}. The position of z=R_a is expressed by the value L_a. The absolute value and the phase for the mutual coupling terms S_{a12} and S_{a21} are fixed to the above mentioned simulated values of 0.017 and 69°, respectively. Operation is assumed to be conducted mainly on the arrow ranged from 0.78 to 5.7 Ω in the figures. Fig. 8(a) shows the phase difference between top and bottom antenna heads estimated with the phases of forward waves into the both antenna heads, that is, phase of V_{f_bottom}/V_{f_top}. It was found that the phase difference changes drastically depending on the loading resistance. Since the two antenna heads are located vertically, the effect of drastic change of phase on the wave number parallel to the static magnetic field $k_{//}$ is small and the heating performance is expected to be maintained constant. Fig. 8(b) shows the absolute value of the reflection coefficient γ at the input port of CIA, that is, $|V_r/V_f|$ assuming the impedance matching is conducted at the loading resistance of 1.25 and 5.0 Ω on the arrow with a loss-less impedance matching device. The calculation was conducted with the following equation (see Appendix B):

$$|\gamma| = \left| \frac{z - R_m}{z + R_m} \right|, \tag{4}$$

where R_m (real number) is the impedance at the bottom of voltage distribution in the line connected to port 3 in Fig. 3 at the matching conditions of S_a=S_{a1} and S_a=S_{a2}. The character z means the impedance at the same position on the line at the arbitrary S_a. In the wide region of R_a-L_a space, the reflection coefficient is kept low.

2.5 Ceramic feedthrough and ex-vessel impedance matching unit

As shown in Fig. 1(b), the LHD type ceramic feedthrough was inserted at the boundary between the vacuum and the pressurized region. The outer conductor of the feedthrough can be water-cooled. The inner conductor in the vacuum side of the ceramic feedthrough has a large diameter for the reduction of the voltage at the feedthrough. The ex-vessel region must also be compact to keep the space for the pathway behind the CIA. Therefore, an ex-vessel impedance transformer (EVIT) [15] is inserted to enhance capacitance, and a stub with a thin inner conductor is used to enhance inductance. Position and size of these parts are determined to make the reflection zero at the two matching points, that is, S_a=S_{a1} and S_a=S_{a2}. Since the reflection is kept low in the wide region of R_a-L_a space as shown in Fig. 8(b), other tunable matching devices are not necessary. For the heat removal from the end of ceramic feedthrough, a thin stainless pipe for cooling water is inserted into the inside of the inner conductor from the end of the stub as shown in Fig. 1(b). Returned cooling water removes generated heat on the inner conductor in the ex-vessel region. Though the inner conductor in in-vessel region is not directly water-cooled in order to reduce the risk of the water leakage, the heat caused by the current mainly generated around the junction unit is removed from the end of the ceramic feedthrough and the antenna head with the thermal conductivity.

3. Simulation results of electric field at various operation points

The electromagnetic simulations were conducted using HFSS in order to investigate the risk of arcing caused by the large amplitude of electric field. For the investigation of the whole electric field except for that on the antenna heads, S-matrix of antenna heads S_a was scanned at the following assumed operation points on the arrows in Fig. 8(a) and (b):

(a) Minimum loading resistance: R_a=0.78 Ω
(b) Lower loading resistance for matching: R_a=1.25 Ω
(c) Loading resistance of typical plasma: R_a=1.7 Ω

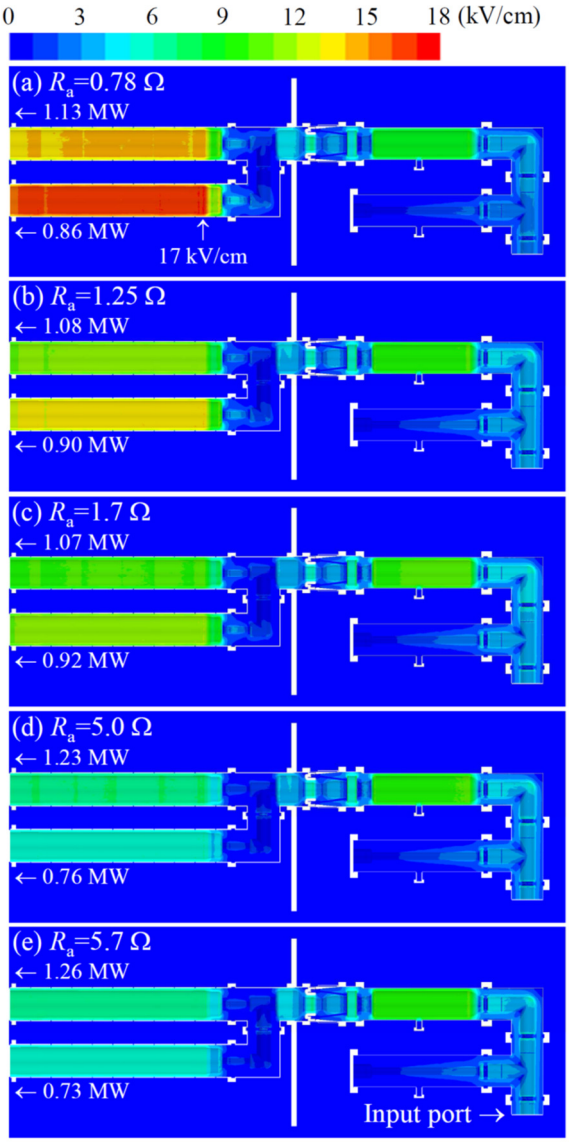

Fig. 9 The amplitude of the electric field at the assumed operation points of (a) the minimum loading resistance, (b) the lower loading resistance for the impedance matching, (c) the loading resistance for the typical plasma, (d) the higher loading resistance for the impedance matching, and (e) the maximum loading resistance.

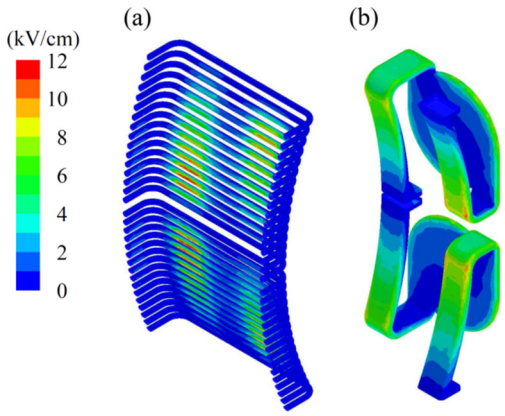

Fig. 10 The amplitude of the electric field on (a) the Faraday shields and (b) the straps in the case of the injection into the pseudo plasma (ε_r=1.0×10^3).

(d) Higher loading resistance for matching: R_a=5.0 Ω
(e) Maximum loading resistance: R_a=5.7 Ω

For the electromagnetic simulation with the arbitrary S_a, at first, the S-matrix with 3×3 elements of the system from the input port of CIA to the output ports of impedance transformers S was calculated with HFSS, and the incident waves into the three ports were adjusted using the designated S-matrix of antenna heads S_a with the calculation method mentioned in Appendix C. Fig. 9(a) to (e) show the amplitude of the electric field in the CIA except for antenna heads at the above mentioned operation points. The forward power at the input port is 2 MW. In the typical case, the amplitude of electric field is less than 13 kV/cm. When the loading resistance of antenna heads R_a decreases, the amplitude of the electric field increases until utmost 17 kV/cm. However, the amplitude of the electric field is still smaller than the specification of the amplitude of the electric field in the ICRF antenna for ITER of 20 kV/cm in the direction of static magnetic field [16]. The injection powers into top and bottom antenna heads indicated with arrows are different from each other. The imbalance of the injection powers is caused by the existence of mutual coupling terms S_{a12} and S_{a21} and the variation of L_a. In addition, the impedance transformers between the antenna heads and the T-junction also cause the imbalance in the injection powers.

The amplitude of the electric field around antenna heads was also simulated in the case of the injection into the pseudo plasma (ε_r=1.0×10^3, plasma~limiter=1 cm, R_a=1.7 Ω) with the forward power of 2 MW at the input port of CIA, where the estimated reflected power is 18.5 kW. The simulated maximum electric field in antenna heads was approximately 12 kV/cm at the backside of Faraday shields as shown in Fig. 10(a) and the second largest electric field was approximately 11 kV/cm in front of straps as shown in Fig. 10(b). Since the directions of these electric fields are almost perpendicular to the static magnetic field line, the risk of arcing caused by the electric field on the Faraday shields are considered low even with lower R_a.

4. Summary

We developed a compact ICRF antenna CIA for ICRF heating with the expected injection power of 2 MW for 300 s in the KSTAR. For the load resilience and the compactness, design method of the generalized conjugate-T with the optimized impedance transformers was developed. As a result, a compact conjugate-T system was successfully designed. A compact ex-vessel impedance matching unit was also designed by using the EVIT and the stub where the capacitance and the inductance are enhanced, respectively. In order to minimize the risk of water leakage, only the backsides of antenna heads are water-cooled in the in-vessel region. The fabrication of CIA has been completed. It will be installed in the KSTAR and the initial injection tests will be performed in the KSTAR campaign.

Acknowledgments

The authors thank staff members in VITZRO Tech for the detail design and the fabrication of the CIA. This research project was financially supported by the Korean Ministry of Science and ICT for the KSTAR project (Grant ID: NFRI-EN1901).

Appendix A

The admittance y at the port 3 shown in Fig. 3 can be calculated with the S-matrices of components. First of all, admittance matrix (Y-matrix) of the system consisted of antenna heads, impedance transformers and extra lines Y_A, and the Y-matrix of the junction unit Y_B should be calculated from the S-matrices of the components. Then, the relation between currents and voltages at the ports are written as follows:

$$\begin{cases} \begin{pmatrix} I_{A1} \\ I_{A2} \end{pmatrix} = Y_A \begin{pmatrix} V_1 \\ V_2 \end{pmatrix} \\ \begin{pmatrix} I_{B1} \\ I_{B2} \\ I_{B3} \end{pmatrix} = Y_B \begin{pmatrix} V_1 \\ V_2 \\ V_3 \end{pmatrix} \end{cases}. \tag{5}$$

These currents are added as follows:

$$\begin{pmatrix} I_1 \\ I_2 \\ I_3 \end{pmatrix} = \begin{pmatrix} I_{A1} \\ I_{A2} \\ 0 \end{pmatrix} + \begin{pmatrix} I_{B1} \\ I_{B2} \\ I_{B3} \end{pmatrix} = Y \begin{pmatrix} V_1 \\ V_2 \\ V_3 \end{pmatrix}, \tag{6}$$

where

$$Y = \begin{pmatrix} Y_{A11} + Y_{B11} & Y_{A12} + Y_{B12} & Y_{B13} \\ Y_{A21} + Y_{B21} & Y_{A22} + Y_{B22} & Y_{B23} \\ Y_{B31} & Y_{B32} & Y_{B33} \end{pmatrix}. \tag{7}$$

Eq. (6) can be rewritten using the impedance matrix Z:

$$\begin{pmatrix} V_1 \\ V_2 \\ V_3 \end{pmatrix} = Z \begin{pmatrix} I_1 \\ I_2 \\ I_3 \end{pmatrix}, \tag{8}$$

where

$$Z = Y^{-1}. \tag{9}$$

Because of the current conservation, $I_1 = I_2 = 0$, the following equations are derived:

$$\begin{cases} V_1 = Z_{13} I_3 \\ V_2 = Z_{23} I_3 \\ V_3 = Z_{33} I_3 \end{cases}. \tag{10}$$

Therefore, the admittance y is determined as follows:

$$y = 1 / Z_{33}. \tag{11}$$

Appendix B

The loss-less impedance matching device with the S-matrix of S_m defined with the port impedance of R_m (real number) for the port 2 (the output port of the impedance matching device) is assumed to be connected at the point where the impedance is R_m on a transmission line. Then, the reflection ratio at the port 1 (input port of the impedance matching device) is assumed to be zero. That is, S_{m11} is zero. Equations $|S_{m12}|=|S_{m21}|=1$ and $S_{m22}=0$ are derived with the condition that there is no energy dissipation in the impedance matching device, that is, S_m is a unitary matrix. When the output impedance changes from R_m to z, the reflection ratio at the port 2 γ_2 is written with the following equation by using the characteristic impedance of R_m:

$$\gamma_2 = \frac{z - R_m}{z + R_m}. \tag{12}$$

The reflection ratio at the port 1 γ is calculated with the S-matrix of S_m as follows:

$$\gamma = S_{m12} S_{m21} \gamma_2. \tag{13}$$

Therefore, the following equations are derived:

$$|\gamma| = \left| \frac{z - R_m}{z + R_m} \right|. \tag{14}$$

Appendix C

Incident wave into each port of the system from the input port of CIA to the output ports of the impedance transformers with the S-matrix of S (3×3 elements) can be calculated with the arbitrary S-matrix of antenna heads S_a (2×2 elements). The incident waves into the ports of the system with the S-matrix of S and the scattered waves defined as shown in Fig. 11 have the following relation:

$$\begin{pmatrix} b_1 \\ b_2 \\ b_3 \end{pmatrix} = S \begin{pmatrix} a_1 \\ a_2 \\ a_3 \end{pmatrix}. \tag{15}$$

For the system of antenna heads with the S-matrix of S_a, the relation is written as follows:

$$\begin{pmatrix} a_1 \\ a_2 \end{pmatrix} = S_a \begin{pmatrix} b_1 \\ b_2 \end{pmatrix}. \tag{16}$$

From the Eq. (15), the following equation is derived assuming a_3=1:

$$\begin{pmatrix} b_1 \\ b_2 \end{pmatrix} = S' \begin{pmatrix} a_1 \\ a_2 \end{pmatrix} + \begin{pmatrix} S_{13} \\ S_{23} \end{pmatrix}, \tag{17}$$

where

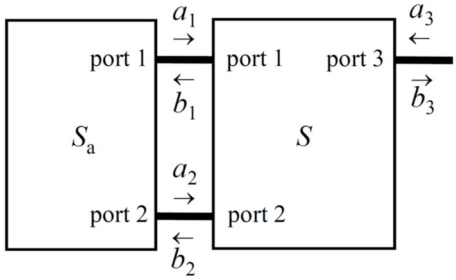

Fig. 11 Definition of the waves at three ports.

$$S' = \begin{pmatrix} S_{11} & S_{12} \\ S_{21} & S_{22} \end{pmatrix}. \quad (18)$$

By using Eqs. (16) and (17), the following equation is derived:

$$\begin{pmatrix} b_1 \\ b_2 \end{pmatrix} = (I - S'S_a)^{-1} \begin{pmatrix} S_{13} \\ S_{23} \end{pmatrix}. \quad (19)$$

From Eq. (15), the scattered wave b_3 is also determined as follows:

$$b_3 = S_{31}a_1 + S_{32}a_2 + S_{33}, \quad (20)$$

where the incident waves a_1, a_2 are derived with Eq. (16) by using the obtained values of b_1 and b_2 with Eq. (19). Therefore, all incident and scattered waves are determined with the condition of a_3=1. Finally, these waves should be modified with the designated power.

References

[1] J.G. Kwak, Y.K. Oh, H.L. Yang, K.R. Park, Y.S. Kim, et al., Nucl. Fusion 53 (2013) 104005.
[2] Y.D. Bae, J.G. Kwak, S.K. Kim, J.S. Yoon, B.G. Hong, et al., Nucl. Fusion 43 (2003) 805-811.
[3] S.J. Wang, H.J. Kim, J.H. Kim, B.H. Park, S.H. Kim, J.G. Kwak, et al., Fusion Eng. Des. 101 (2015) 22-27.
[4] J.G. Kwak, S.J. Wang, J.S. Yoon, Y.D. Bae, S.K. Kim, et al., Fusion Eng. Des. 84 (2009) 1140-1143.
[5] J.G. Kwak, S.J. Wang, J.S. Yoon, Y.D. Bae, B.G. Hong, et al., J. Korean Phys. Soc. 49 (2006) S305-S308.
[6] I. Monakhov, T. Blackman, A. Walden, M. Nightingale, A. Whitehurst, et al., Proc. of 15th Top. Conf. on RF Power in Plasmas 694 (2003) 150-151.
[7] J.G. Kwak, S.K. Kim, C.K. Hwang, Y.D. Bae, J.S. Yoon, et al., Proc. of 17th Top. Conf. on RF Power in Plasmas 933 (2007) 179-182.
[8] Y. Takeiri, T. Morisaki, M. Osakabe, M. Yokoyama, S. Sakakibara, et al., Nucl. Fusion 57 (2017) 102023.
[9] K. Saito, R. Kumazawa, T. Seki, H. Kasahara, M. Osakabe, et al., Fusion Sci. Technol. 58 (2010) 515-523.
[10] K. Saito, T. Mutoh, R. Kumazawa, T. Seki, Y. Nakamura, et al., J. Nucl. Mater. 363-365 (2007) 1323-1328.
[11] R. Kumazawa, T. Mutoh, K. Saito, T. Seki, H. Kasahara, et al., Fusion Sci. Technol. 58 (2010) 524-529.
[12] T. Mutoh, R. Kumazawa, T. Seki, F. Simpo, G. Nomura, et al., Fusion Technol. 35 (1999) 297-308.
[13] K. Saito, T. Seki, H. Kasahara, R. Seki, S. Kamio, et al., Fusion Eng. Des. 96-97 (2015) 583-588.
[14] K. Saito, T. Seki, H. Kasahara, R. Seki, R. Kumazawa, et al., Fusion Eng. Des. 88 (2013) 1025-1029.
[15] K. Saito, T. Seki, H. Kasahara, R. Seki, S. Kamio, et al., J. Phys.: Conf. Ser. 823 (2017) 012007.
[16] M. Vrancken, F. Durodié, P. Dumortier, D. Lockley, F. Louche, et al., Proc. of 19th Top. Conf. on RF Power in Plasmas 1406 (2011) 61-64.